

# Phase-space interference of states optically truncated by quantum scissors: Generation of distinct superpositions of qudit coherent states by displacement of vacuum

Adam Miranowicz,<sup>1,2</sup> Małgorzata Paprzycka,<sup>1</sup> Anirban Pathak,<sup>3,4</sup> and Franco Nori<sup>2,5</sup><sup>1</sup>*Faculty of Physics, Adam Mickiewicz University, PL-61-614 Poznań, Poland*<sup>2</sup>*CEMS, RIKEN, Saitama 351-0198, Japan*<sup>3</sup>*Department of Physics and Materials Science and Engineering, JIIT, A-10, Sector-62, Noida, UP-201307, India*<sup>4</sup>*RCPTM, Joint Laboratory of Optics of Palacký University and Institute of Physics of Academy of Science of the Czech Republic, Faculty of Science, Palacký University, 771 46 Olomouc, Czech Republic*<sup>5</sup>*Physics Department, The University of Michigan, Ann Arbor, Michigan 48109-1040, USA*

(Received 26 July 2013; published 10 March 2014)

Conventional Glauber coherent states (CS) can be defined in several equivalent ways, e.g., by displacing the vacuum or, explicitly, by their infinite Poissonian expansion in Fock states. It is well known that these definitions become inequivalent if applied to finite  $d$ -level systems (qudits). We present a comparative Wigner-function description of the qudit CS defined (i) by the action of the truncated displacement operator on the vacuum and (ii) by the Poissonian expansion in Fock states of the Glauber CS truncated at  $(d - 1)$ -photon Fock state. These states can be generated from a classical light by its optical truncation using nonlinear and linear quantum scissors devices, respectively. We show a surprising effect that a macroscopically distinguishable superposition of two qudit CS (according to both definitions) can be generated with high fidelity by displacing the vacuum in the qudit Hilbert space. If the qudit dimension  $d$  is even (odd), then the superposition state contains Fock states with only odd (even) photon numbers, which can be referred to as the odd (even) qudit CS or Schrödinger's cat state. This phenomenon can be interpreted as an interference of a single CS with its reflection from the highest-energy Fock state of the Hilbert space, as clearly seen via phase-space interference of the Wigner function. We also analyze nonclassical properties of the qudit CS including their photon-number statistics and nonclassical volume of the Wigner function, which is a quantitative parameter of nonclassicality (quantumness) of states. Finally, we study optical tomograms, which can be directly measured in the homodyne detection of the analyzed qudit cat states and enable the complete reconstructions of their Wigner functions.

DOI: [10.1103/PhysRevA.89.033812](https://doi.org/10.1103/PhysRevA.89.033812)

PACS number(s): 42.50.Dv, 42.50.Gy

## I. INTRODUCTION

Coherent states (CS), since their original introduction by Schrödinger [1], Glauber [2], and Sudarshan [3], have been playing a central role in quantum physics [4,5], including quantum and atom optics, mathematical physics, solid-state physics (e.g., theories of superconductivity), quantum field theory, and string theory. The conventional infinite-dimensional bosonic CS are the most classical pure quantum states of the quantum harmonic oscillator. The importance of CS can be clearly seen through the Wigner or, equivalently, Glauber-Sudarshan formalisms of quantum mechanics based on quasiprobabilities in phase space [6]. Much effort, including the works of Perelomov [7] and Gilmore (as reviewed in Ref. [4]), has been focused on generalizations of CS for finite-dimensional bosonic or fermionic CS.

Here we study qudit coherent states (QCS), i.e., finite-dimensional analogs of the conventional infinite-dimensional Glauber CS [8–16] (for a review see [17]). QCS were studied since the 1990s in the context of quantum phase problems (especially for the Pegg-Barnett formalism; for reviews see [18,19]), and quantum information and engineering (reviewed in, e.g., Refs. [20–22]) in qudit systems.

In general, qudit states defined in Hilbert space  $\mathcal{H}^{(d)}$  of a finite dimension  $d$  can be expanded in the Fock-state  $|n\rangle$  basis as

$$|\psi\rangle_d = \sum_{n=0}^{d-1} c_n |n\rangle, \quad (1)$$

where  $c_n$  are the properly normalized superposition coefficients. In the special cases for  $d = 2, 3, 4$ , the states  $|\psi\rangle_d$  are often referred to as the qubit, qutrit, and quartit (or ququart) states, respectively.

Quantum information processing with qudits has some practical advantages over that with qubits as it could speed up certain computing tasks, by simplifying logic gates [23–25], improving quantum cryptography [26], and using physical resources more efficiently [27]. Experimental demonstrations of quantum information processing with qudits include quadrupolar nuclear spins (i.e., quartits) controlled with nuclear magnetic resonance in bulk liquids [28], bulk solids [29], and semiconductor quantum wells [27], as well as superconducting phase qudits with a number of levels  $d$  up to five [30], and photonic qutrits in linear optical architectures [25]. Optical qudit states can be physically generated from infinite-dimensional states by optical state truncation using the so-called quantum scissors devices [20,22]. Simple examples of such scissors are shown in Fig. 1.

Various nonclassical properties of qudit states were investigated on several occasions. Interestingly, the states are referred to by different names depending on the functional form of  $c_n$ . We are in general interested in the nonclassical properties of the quantum state described by Eq. (1). However, the present study would be focused on the QCS.

The conventional infinite-dimensional Glauber CS  $|\alpha\rangle$  of light can be defined in several equivalent ways. For example, (i) by the action of the displacement operator

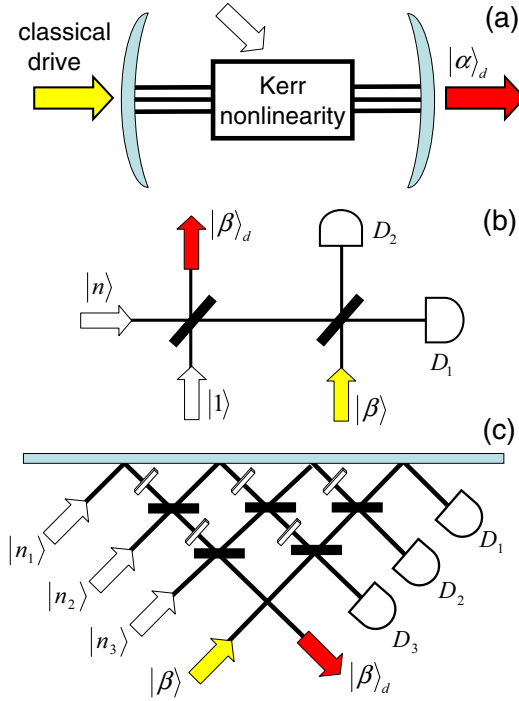


FIG. 1. (Color online) Examples of (a) nonlinear and [(b),(c)] linear quantum scissors devices for the generation of the QCS if losses are negligible. Yellow (red) arrows denote input (output) fields, white arrows are auxiliary fields, solid bars correspond to beam splitters, blue bars to mirrors, empty bars to phase shifters, and  $D_n$  are photodetectors. (a) A cavity with a Kerr medium ( $d$ -photon anharmonic oscillator), described by a nonlinear coupling proportional to the  $(2d - 1)$ th-order nonlinear susceptibility, driven by a classical laser light enables, in principle, a deterministic generation of the QCS  $|\alpha\rangle_d$  [12] (for  $d = 2$  see Ref. [48] for details). (b) The Pegg-Phillips-Barnett scissors [61] for the probabilistic generation (i.e., projection synthesis) of the QCS  $|\beta\rangle_d$  with  $d = 2, 3$  via optical truncation and quantum teleportation of the incident CS  $|\beta\rangle$  conditioned on the proper photon-number detection at the detectors  $D_n$  using beam splitters with proper transmission and reflection parameters, and the auxiliary Fock states  $|1\rangle$  and  $|n\rangle$  ( $n = 0$  for  $d = 2$  and  $n = 1$  for  $d = 3$ ). (c) A generalized version of the Pegg-Phillips-Barnett scissors based on a generalized Mach-Zehnder interferometer for a probabilistic optical truncation and teleportation of  $|\beta\rangle$  to the QCS  $|\beta\rangle_d$  with  $d = 2, \dots, 6$  [62]. Note that the configuration (c) is scalable for arbitrary  $d$ . It should be stressed that the generation of QCS described here can be realized also in various other bosonic finite-dimensional systems (see text).

$\hat{D}(\alpha, \alpha^*) \equiv \exp(\alpha \hat{a}^\dagger - \alpha^* \hat{a})$  on the vacuum state  $|0\rangle$ , where  $\hat{a}$  ( $\hat{a}^\dagger$ ) is the conventional infinite-dimensional annihilation (creation) operator. Equivalently, these CS can be defined by (ii)  $|\alpha\rangle = \mathcal{N} \exp(\alpha \hat{a}^\dagger) |0\rangle$  as implied by the definition (i) but with the displacement operator factorized according to the Campbell-Baker-Hausdorff theorem. Hereafter, the function  $\mathcal{N}$  normalizes a given state  $|\psi\rangle$ , i.e.,  $\mathcal{N}|\psi\rangle = |\psi\rangle / \sqrt{\langle\psi|\psi\rangle}$ . These equivalent definitions of the infinite-dimensional CS become inequivalent if applied to the finite-dimensional Hilbert spaces, as will be shown in detail in this paper.

Optical Schrödinger cat states have attracted both theoretical [6,31] and experimental [32] interest in quantum optics,

quantum engineering, and quantum information processing with continuous variables.

Here we describe how to generate superpositions of macroscopically distinct QCS (i.e., Schrödinger-cat-like states) by the displacement of the vacuum in a Hilbert space for qudits. We explain this counterintuitive result physically, in terms of interference in phase space, and analytically by recalling the properties of the roots of the Hermite polynomials. These cat states are finite-dimensional analogs of the even and odd infinite-dimensional CS. Some preliminary results, concerning the generation of even QCS, were obtained in Ref. [33] (see also the review [17]) but without a complete analytical proof and a deeper physical explanation. Moreover, the generation of odd QCS has not been predicted so far.

Wigner's [34] formulation of quantum mechanics based on quasiprobabilities in phase space is completely equivalent to other quantum formalisms including those of Schrödinger and Heisenberg albeit *without* the use of wave functions and operators [35]. The Wigner function is useful in quantum optics [6] in describing, e.g., interference in phase space, and can be directly measured [36,37] or indirectly reconstructed using homodyne tomography both for infinite- [6] and finite-dimensional [38] systems.

In this paper, we apply the Wigner function formalism to study both the interference in phase space and the homodyne detection of QCS. Note that a nonstandard finite-dimensional Wigner function [39,40] defined on a torus was already applied to study some properties of QCS in Refs. [17,33]. By contrast, here we apply the standard Wigner function which, arguably, is simpler for physical interpretations and for its measurement if the Hilbert-space dimension is not very small or is unspecified.

Thus, we describe here nonclassical properties of the qudit cat states revealed in their Wigner functions. In particular, we analyze the nonclassical volume of the Wigner function, which is a quantitative parameter of nonclassicality [41].

We also discuss optical tomograms, which can be directly measured in the homodyne detection of the analyzed cat states.

This paper is organized as follows: In Secs. II and III, we present two different constructions of QCS. We also describe their Wigner representations and methods for their generation. In Sec. IV we show the main result of this paper: that the QCS defined by the displacement of the vacuum can almost periodically become the Schrödinger cat states having a clear interpretation in terms of the Wigner function. We conclude in Sec. V.

## II. QUDIT COHERENT STATES BY DISPLACEMENT OF VACUUM

### A. Definition and Fock-state expansion

In analogy to the first Glauber definition of the infinite-dimensional CS, mentioned in the Introduction, one can construct a QCS by applying a qudit displacement operator to the vacuum [8]:

$$|\alpha\rangle_d = \hat{D}_d(\alpha, \alpha^*) |0\rangle = \exp(\alpha \hat{a}_d^\dagger - \alpha^* \hat{a}_d) |0\rangle, \quad (2)$$

where the qudit annihilation operator is defined by

$$\hat{a}_d = \sum_{n=1}^{d-1} \sqrt{n} |n-1\rangle \langle n| \quad (3)$$

and  $\hat{a}_d^\dagger$  is the qudit creation operator, which are the truncated versions of the usual infinite-dimensional annihilation and creation operators, respectively. We note that the commutator

$$[\hat{a}_d, \hat{a}_d^\dagger] = 1 - d|d-1\rangle\langle d-1| \quad (4)$$

is a quantum number, which fundamentally differs from the canonical commutation relation for the standard annihilation  $\hat{a}$  and creation  $\hat{a}^\dagger$  operators. This mathematical property implies that quantum interference in phase space of the QCS is completely different from that of the standard coherent states, as will be described in detail in the next sections.

The Fock-state expansion of the QCS  $|\alpha\rangle_d$  is much more complicated than that for conventional CS and given by [10]

$$|\alpha\rangle_d = \sum_{n=0}^{d-1} c_n^{(d)}(\alpha) |n\rangle \quad (5)$$

with the superposition coefficients

$$c_n^{(d)}(\alpha) = f_n^{(d)} \sum_{k=0}^{d-1} \frac{\text{He}_n(x_k)}{[\text{He}_{d-1}(x_k)]^2} \exp(ix_k|\alpha|), \quad (6)$$

where

$$f_n^{(d)} = \frac{(d-1)!}{d} (n!)^{-1/2} \exp\left[in\left(\phi_0 - \frac{\pi}{2}\right)\right] \quad (7)$$

and  $\text{He}_n(x)$  is the modified Hermite polynomial simply related to the standard Hermite polynomial  $H_n(x)$  as

$$\text{He}_n(x) = 2^{-n/2} H_n(x/\sqrt{2}). \quad (8)$$

Moreover,  $x_k \equiv x_k^{(d)}$  is the  $k$ th root of  $\text{He}_d(x)$ , and  $\phi_0 = \arg(\alpha)$ . For  $d=2$ , the general formula, given by Eqs. (5) and (6), reduces to

$$|\alpha\rangle_2 = \cos(|\alpha|)|0\rangle + e^{i\phi_0} \sin(|\alpha|)|1\rangle, \quad (9)$$

which shows that any single-qubit pure state can be considered this QCS for a proper choice of  $\alpha$ . Of course, this is not the case for dimensions  $d > 2$ . Two nontrivial examples for the qutrit CS  $|\alpha\rangle_3$  and quartit CS  $|\alpha\rangle_4$  are given in the Appendix.

Any finite superposition of Fock states, thus in particular the QCS  $|\alpha\rangle_d$ , can be realized by various experimental methods and systems (see, e.g., Ref. [42]). Here we just mention the experiments of Zeilinger's group [43] using generalized Mach-Zehnder interferometers in a triangular configuration shown in Fig. 1(c), and those of the Martinis group [44] using microwave resonators coupled to superconducting quantum circuits [45]. It is also worth noting a probabilistic method proposed in Ref. [46], which uses a cross-Kerr medium coupled to a ring cavity to synthesize arbitrary superpositions of Fock states. Unfortunately, this method is based on *probabilistic* projective measurements contrary to the method described below.

Let us now briefly describe the completely different approach of Ref. [12], shown schematically in Fig. 1(a). This method enables, in principle, a direct and *deterministic* dynamical generation of the QCS  $|\alpha\rangle_d$  for any amplitude  $\alpha$  and small dimensions  $d$ . This is achieved by optical-state truncation of the incident classical field by the so-called nonlinear quantum scissors device composed of a higher-order Kerr medium (modeled as a  $d$ -photon anharmonic oscillator) in a cavity pumped by a classical driving field [12]. For this

reason, the QCS  $|\alpha\rangle_d$  is sometimes referred to as the *nonlinear* QCS.

This optical truncation in the special case for  $d=2$  results in the celebrated single-photon blockade [47,48], which is an effect when a single photon in a cavity with a Kerr nonlinearity blocks the excitation of more photons in the cavity field. The Kerr nonlinearity (which is proportional to the third-order nonlinear susceptibility) can be induced relatively easily by a strong interaction between the cavity field and natural or artificial qubit [49–51], which might be a single trapped atom [52], a quantum dot [53], or a superconducting artificial atom [54,55]. The single-photon blockade has been mainly studied in the systems of cavity quantum electrodynamics (QED) including theoretical predictions (see, e.g., Ref. [56]) and experimental demonstrations [52,53]. Recently, impressive experimental progress was also reported in circuit-QED systems [54,55]. Note that the two- and three-photon blockades can be, in principle, observed in these systems where the single-photon blockade was measured, but with the choice of different resonance conditions [57]. Other generalized blockade effects comprise two-mode optical state truncation [58] and single-*phonon* blockade [59,60].

## B. Wigner representation of displaced vacuum for qudits

The Wigner function associated with an arbitrary single-mode state  $\rho$  is defined by [34]

$$W(z) \equiv W_\rho(q, p) = \frac{1}{\pi} \int \langle q-x|\rho|q+x\rangle \exp(2ipx) dx, \quad (10)$$

where  $q$  and  $p$  are the canonical position and momentum operators, respectively, and  $z = q + ip$ .

The concept of quantum interference in phase space for finite superpositions of Fock states (so, in particular, for our QCS) can be clearly explained in terms of the Wigner function [31,63], which will be discussed below. Alternatively, one could explain this interference in a semiclassical picture of the areas of overlap (i.e., interfering areas) [6,64]. Here we follow the completely quantum approach of Ref. [31].

The Wigner function for a qudit state, defined by Eq. (1), can be given as a sum of two terms,

$$W(z) = W_{\text{mix}}(z) + W_{\text{int}}(z), \quad (11)$$

representing, respectively, the noninterference (or mixture) part for the Wigner function

$$W_{\text{mix}}(z) = \sum_{n=0}^{d-1} |c_n|^2 W_n(z), \quad (12)$$

which is given as a sum of the Wigner functions of the Fock states  $|n\rangle$ ,

$$W_n(z) = \frac{2}{\pi} (-1)^n \exp(-2|z|^2) L_n(4|z|^2), \quad (13)$$

and the interference part

$$W_{\text{int}}(z) = 2 \sum_{k < l}^{d-1} \text{Re}[c_k^* c_l W_{kl}(z)], \quad (14)$$

where

$$W_{kl}(z) = \frac{2}{\pi} (-1)^k \sqrt{\frac{k!}{l!}} (2z^*)^{l-k} e^{-2|z|^2} L_k^{(l-k)}(4|z|^2), \quad (15)$$

and  $L_k^{(l-k)}(x)$  are the associated Laguerre polynomials with  $L_k(x) \equiv L_k^{(0)}(x)$ . Equation (14) can be rewritten more compactly as

$$W_{\text{int}}(z) = \frac{4}{\pi} e^{-2|z|^2} \sum_{k < l} (-1)^k |c_k| |c_l| \sqrt{\frac{k!}{l!}} (2|z|)^{l-k} \times L_k^{(l-k)}(4|z|^2) \cos(\Phi_{kl}), \quad (16)$$

where  $\Phi_{kl} = \arg(c_k^*) + \arg(c_l) + (k - l)\arg(z)$ .

It is seen that  $W_{\text{mix}}(z)$  and  $W_{\text{int}}(z)$  correspond, respectively, to the diagonal and off-diagonal terms of the density matrix  $\rho = |\psi\rangle\langle\psi|$  in Fock basis. The Wigner function is *phase insensitive* for Fock states  $|n\rangle$  (for any  $n$ ) and their mixtures, so  $W_{\text{mix}}(z)$  is symmetric for any rotations around  $z = 0$ . By contrast, a superposition of Fock states can be *phase sensitive* as described by the interference part  $W_{\text{int}}(z)$  of the Wigner function, which explicitly depends on the phases  $\Phi_{kl}$  (for  $k \neq l$ ), although the corresponding component Fock states  $|k\rangle$  and  $|l\rangle$  are phase insensitive. Thus, interference of probability amplitudes associated with off-diagonal terms of a density matrix can be clearly described via interference in phase space, although the Wigner-function approach is based on probabilities (or rather quasiprobabilities as they can be negative) instead of probability amplitudes.

A few examples of the Wigner function for the qubit CS  $|\alpha\rangle_2$  are shown in Fig. 2, which can be compared with the corresponding Wigner functions, shown in Fig. 3, for another type of the qubit CS defined below. The Wigner functions for the qutrit CS  $|\alpha\rangle_3$  are shown in Fig. 4. For clarity, we rescaled colors in the plots of the Wigner functions such that dark blue (dark red) corresponds to the minimum (maximum) values in each figure. Blue regions correspond to the negative values of the Wigner functions, which are the indicators of nonclassicality of the states. Moreover, the black outer circles in these figures show the areas in phase space, which are dominantly occupied by the Wigner function for a given qudit state. Tails of the Wigner function outside such circles can be practically ignored. Strictly speaking, the Wigner function occupies the whole phase space for any state, including the vacuum. But, the area where the Wigner function is greater than an arbitrary threshold value is finite. This area of phase space can be chosen arbitrarily. For example, to describe an arbitrary  $d$ -dimensional state, we chose an area large enough to cover the peak of the Wigner of an infinite-dimensional CS  $|\alpha\rangle$  with  $|\alpha|^2 = d - 1$ , which is the photon number of the highest-energy Fock state in  $\mathcal{H}^{(d)}$ , and the radius  $r_0$  corresponding to its half width at half maximum. This  $r_0$  for a Gaussian curve with the standard deviation  $\sigma$  is equal to  $r_0 = \sigma\sqrt{2 \ln 2}$ . The Wigner function for the CS  $|\alpha\rangle$  is  $W_\alpha(q, p) = (2/\pi) \exp(-2|q + ip - \alpha|^2)$ . Thus, the radius of the outer circles in Figs. 2–6 was chosen as

$$r = \sqrt{d-1} + \sqrt{\ln 2/2}. \quad (17)$$

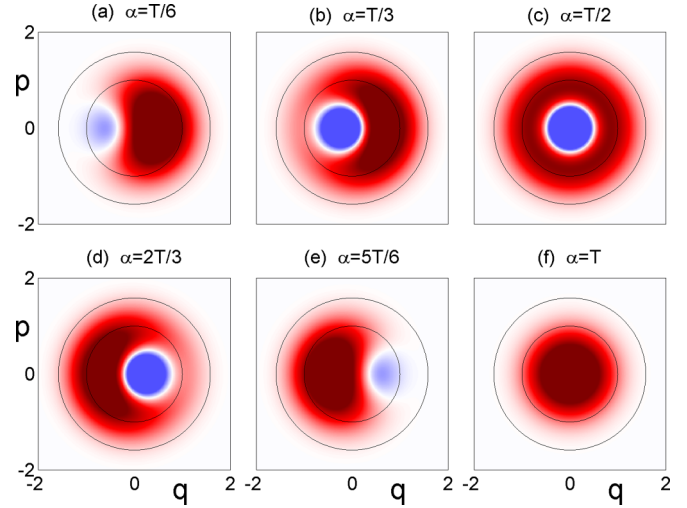


FIG. 2. (Color online) Wigner functions for the qubit CS  $|\alpha\rangle_2$  and various values of the real amplitude  $\alpha = nT/6$ , where  $T = T_2 = \pi$ . Note the snapshots of the oscillations and the interference fringes in the Wigner function. The increase of  $\alpha$  can be interpreted as the evolution of the driven Kerr system, shown in Fig. 1(a), assuming negligible dissipation. The negative (positive) regions of the Wigner function are marked in blue (red), with the deeper color the more extreme values. Zero corresponds to white color. The inner and outer circles have radii given by  $r = \sqrt{d-1}$  and Eq. (17), respectively. It is seen that the Wigner functions are practically vanishing beyond the outer circles. Panels (c) and (f) show the Wigner functions for the single-photon and vacuum states, respectively. The Wigner functions shown in panels (a), (b), (d), and (e) are phase sensitive, which is a result of quantum interference in phase space.

By comparison, the inner circles in the plots of the Wigner functions have the radius given by  $r = \sqrt{d-1}$ .

It is seen that the QCS  $|\alpha\rangle_d$  with increasing  $\alpha$  (corresponding to evolution time) is reflected from the boundary states  $|0\rangle$  and  $|d-1\rangle$  of the Hilbert space  $\mathcal{H}^{(d)}$ . This phenomenon of multiple reflections (multiple bounce) can be interpreted as a ping-pong effect, which leads, in particular, to the generation of the Schrödinger cat states as will be shown in Sec. IV.

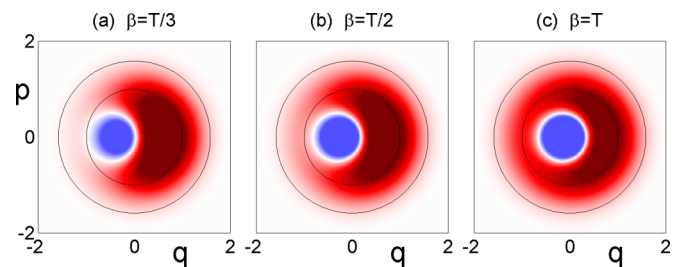


FIG. 3. (Color online) As in Figs. 2(b), 2(c), and 2(f) but for the qubit CS  $|\beta\rangle_2$ . Note that the Wigner function for  $|\beta = T/6\rangle_2$  resembles that for  $|\alpha = T/6\rangle_2$ , as shown in Fig. 2(a), while for  $|\beta = 2T/3\rangle_2$  and  $|\beta = 5T/6\rangle_2$  interpolates between those in panels (b) and (c), where  $T = T_2$ . For brevity, these three figures, corresponding to the cases shown in Figs. 2(a), 2(d), and 2(e), are omitted. In the limit of  $\beta \rightarrow \infty$ , the state  $|\beta\rangle_2$  goes into the single-photon Fock state described by the standard rotationally invariant Wigner function.

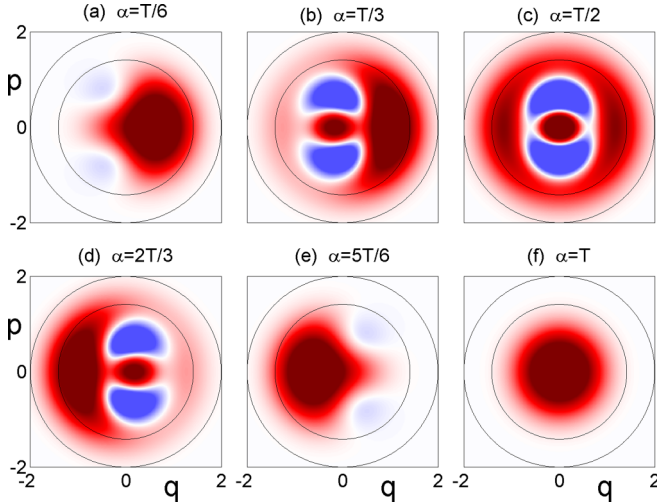


FIG. 4. (Color online) Wigner functions for the qutrit ( $d = 3$ ) CS  $|\alpha\rangle_3$  with  $\alpha = nT_3/6$  with  $n=1,2,\dots$ . The color codes and circles correspond to those in Fig. 2. Panels (c) and (f) show the Wigner functions for a cat state (even QCS) and the vacuum, respectively.

### III. QUDIT COHERENT STATES BY TRUNCATION OF FOCK-STATE EXPANSION OF GLAUBER COHERENT STATES

Another type of the QCS can be simply obtained by truncating the Fock-state superposition of the conventional infinite-dimensional CS as was studied by, e.g., Kuang *et al.* [9]. To be precise, this QCS can be defined by

$$|\beta\rangle_d = \mathcal{N} \exp(\beta \hat{a}_d^\dagger) |0\rangle = \mathcal{N} \sum_{n=0}^{d-1} \frac{\beta^n}{\sqrt{n!}} |n\rangle \quad (18)$$

for a complex amplitude  $\beta$ . This definition is postulated in analogy to the second Glauber definition of the conventional CS based on the Campbell-Baker-Hausdorff theorem as follows:

$$e^{\hat{A}+\hat{B}} |0\rangle = e^{\hat{A}} e^{\hat{B}} e^{\hat{C}} |0\rangle = e^{\hat{C}} e^{\hat{A}} |0\rangle = \mathcal{N} \exp(\beta \hat{a}^\dagger) |0\rangle, \quad (19)$$

where  $\hat{A} = \hat{B}^\dagger = \beta \hat{a}^\dagger$ ,  $\hat{C} = -\frac{1}{2}[\hat{A}, \hat{B}]$ , and  $\mathcal{N} = e^{\hat{C}} = \exp(-\frac{1}{2}|\beta|^2)$ . This theorem can be applied to the infinite-dimensional operators since it holds  $[\hat{A}, [\hat{A}, \hat{B}]] = [\hat{B}, [\hat{A}, \hat{B}]] = 0$ . By contrast, the Campbell-Baker-Hausdorff theorem cannot be applied to the finite-dimensional annihilation and creation operators since the double commutators  $[\hat{a}_d, [\hat{a}_d, \hat{a}_d^\dagger]]$  and  $[\hat{a}_d^\dagger, [\hat{a}_d, \hat{a}_d^\dagger]]$  do not vanish, as can be seen by applying Eq. (4). Thus, the two kinds of QCS, as defined by Eqs. (2) and (18), are fundamentally different (except some special cases) exhibiting different quantum interference in phase space, as seen in Figs. 2–6.

One can refer to  $|\beta\rangle_d$  as the *linear* CS for a qudit since it can be simply (but nondeterministically) obtained by linear optical systems called linear quantum scissors, as shown schematically in Figs. 1(b) and 1(c) and described in detail for  $d = 2$  in Refs. [61,65],  $d = 3$  [66], and higher  $d$  [62]. For  $d = 2$ , Eq. (18) reduces to the qubit CS  $|\beta\rangle_2 = \mathcal{N}(|0\rangle + \beta|1\rangle)$ . Although the systems shown in Figs. 1(b) and 1(c) seemingly contain only linear optical elements,

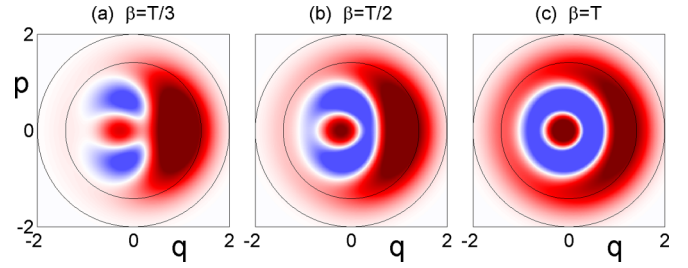


FIG. 5. (Color online) Same as in Figs. 4(b), 4(c), and 4(f) but for the qutrit CS  $|\beta\rangle_3$ . Analogously to Fig. 3, the Wigner function for  $|\beta = T/6\rangle_3$  with  $T = T_3$  resembles that for  $|\alpha = T/6\rangle_3$ , as shown in Fig. 4(a), while for  $|\beta = 2T/3\rangle_3$  and  $|\beta = 5T/6\rangle_3$  interpolates between those in panels (b) and (c). For brevity, these three figures, corresponding to Figs. 4(a), 4(d), and 4(e), are not presented here. Note that the limiting state  $\lim_{\beta \rightarrow \infty} |\beta\rangle_3 = |2\rangle$  is described by the standard rotationally invariant Wigner function of the two-photon Fock state.

the *nonlinearity* is induced by the measurement (i.e., the conditional photodetection). So, the generation of the QCS  $|\beta\rangle_d$  also requires nonlinearity. Nevertheless, the term *linear* QCS stresses only the fact that no nonlinear media are used in the setups of Figs. 1(b) and 1(c).

The Wigner functions for  $|\beta\rangle_2$  are shown in Fig. 3, which could be compared with those for  $|\alpha\rangle_2$  in Fig. 2 for some particular choices of  $\alpha = \beta$ . Analogously, Figs. 4 and 5 of the Wigner functions for the qutrit CS  $|\alpha\rangle_3$  and  $|\beta\rangle_3$ , respectively, show similar properties of the states for  $|\alpha| = |\beta| \ll T_3/2$  [in Figs. 4(b) and 5(a)] and their distinctive properties for other values of  $|\alpha| = |\beta|$  [in Figs. 4(c) and 4(f) and 5(b) and 5(c)].

It is seen that the QCS  $|\beta\rangle_d$  is not reflected from the boundaries of the Hilbert space as  $\beta$  increases. This can be described as ‘no bouncing.’ By contrast, as already mentioned, the QCS  $|\alpha\rangle_d$  exhibits multiple bounce (or a ping-pong effect) as  $\alpha$  increases.

One can define a state  $|\gamma\rangle_d$  complementary to the QCS  $|\beta\rangle_d$ , such that their equally weighted superposition is the QCS:

$$|\alpha\rangle_d = \mathcal{N}(|\beta\rangle_d + |\gamma\rangle_d), \quad (20)$$

which leads to the explicit form of the complementary state

$$|\gamma\rangle_d = 2_d \langle \alpha | \beta \rangle_d |\alpha\rangle_d - |\beta\rangle_d \quad (21)$$

up to a global phase factor. In the simplest case for  $d = 2$ , one can find

$$|\gamma\rangle_2 = \frac{1}{\sqrt{1+\alpha^2}} ([\cos(2\alpha) + \alpha \sin(2\alpha)]|0\rangle + [\sin(2\alpha) - \alpha \cos(2\alpha)]|1\rangle), \quad (22)$$

where for simplicity we assumed  $\alpha$  to be positive. By contrast, the qubit CS  $|\beta\rangle_2$  is given by  $\mathcal{N}(|0\rangle + \beta|1\rangle)$ , as depicted for some choices of  $\beta$  in Fig. 3. Thus, for the choice of  $\alpha = \beta = \gamma = T_2/2$ , we have  $|\gamma\rangle_2 = \mathcal{N}(-|0\rangle + \frac{\pi}{2}|1\rangle) = -|-\beta\rangle_2$ , which results in  $|\alpha\rangle_2 = |1\rangle$ . We note that such a simple relation between  $|\gamma\rangle_d$  and  $|\beta\rangle_d$  exists for  $d = 2$  only. An explicit comparison of  $|\gamma\rangle_d$  and  $|\beta\rangle_d$  for  $d = 3, 4$  is given in the Appendix.

#### IV. CAT-STATE GENERATION

Here we will show one of the main results of this paper: that macroscopically distinguishable superpositions of the QCS (Schrödinger cat states) can be simply generated by displacing the vacuum in the Hilbert space of an optical qudit.

##### A. Even and odd coherent states for qudits

The prototype examples of optical Schrödinger cat states are the even and odd infinite-dimensional CS, defined [31] as  $|\alpha_{\pm}\rangle = \mathcal{N}(|\alpha\rangle \pm |-\alpha\rangle)$ .

By analogy with the infinite-dimensional cat states  $|\alpha_{\pm}\rangle$ , one can define their qudit counterparts as, e.g., the even QCS,  $|\alpha_{+}\rangle_d$ , and odd QCS,  $|\alpha_{-}\rangle_d$ , as follows:

$$|\alpha_{+}\rangle_d = \mathcal{N}(|\alpha\rangle_d + |-\alpha\rangle_d) = \mathcal{N} \sum_{n=0}^{d-1} \frac{c_{2n}^{(d)}(\alpha)|2n\rangle}{\sqrt{(2n)!}}, \quad (23)$$

$$\begin{aligned} |\alpha_{-}\rangle_d &= \mathcal{N}(|\alpha\rangle_d - |-\alpha\rangle_d) \\ &= \mathcal{N} \sum_{n=0}^{d-1} \frac{c_{2n+1}^{(d)}(\alpha)|2n+1\rangle}{\sqrt{(2n+1)!}}, \end{aligned} \quad (24)$$

where the superposition coefficients  $c_n^{(d)}(\alpha)$  are given by Eq. (6). Moreover, one can define other qudit cat states based on the QCS  $|\pm\beta\rangle_d$  as follows:

$$|\beta_{+}\rangle_d = \mathcal{N}(|\beta\rangle_d + |-\beta\rangle_d) = \mathcal{N} \sum_{n=0}^{d-1} \frac{\beta^{2n}|2n\rangle}{\sqrt{(2n)!}}, \quad (25)$$

$$\begin{aligned} |\beta_{-}\rangle_d &= \mathcal{N}(|\beta\rangle_d - |-\beta\rangle_d) \\ &= \mathcal{N} \sum_{n=0}^{d-1} \frac{\beta^{2n+1}|2n+1\rangle}{\sqrt{(2n+1)!}}. \end{aligned} \quad (26)$$

In the following, we will explain why the QCS  $|\alpha\rangle_d$  for  $\alpha = T_d/2$  are very good approximations of either the even QCS  $|\alpha_{+}\rangle_d$  and  $|\beta_{+}\rangle_d$  for odd  $d$  or the odd QCS  $|\alpha_{-}\rangle_d$  and  $|\beta_{-}\rangle_d$  for even  $d$ .

##### B. Periodicity, quasiperiodicity, and symmetries of Wigner functions

As found in Refs. [33,67], the QCS  $|\alpha\rangle_d$  with increasing  $\alpha$  exhibit either perfect periodicity for  $d = 2, 3$  or almost periodicity (“quasiperiodicity”) for  $d > 3$ . The periods for  $d = 2, 3$  are  $T_2 = \pi$  and  $T_3 = 2\pi/\sqrt{3}$ , respectively, while the quasiperiod  $T_d$  for  $d > 3$  is given by

$$T_d = \sqrt{4d+2}. \quad (27)$$

Note that Eq. (27) gives a rough approximation even for  $T_2$  (as  $\pi = \sqrt{10} - 0.02\dots$ ) and  $T_3$  (as  $2\pi/\sqrt{3} = \sqrt{14} - 0.1\dots$ ).

The period  $T_2$  is equal to  $\pi$  up to a global phase since  $|\alpha\rangle_2 = -|\alpha + \pi\rangle_2$  [compare the Wigner function for  $|\alpha = \pi\rangle$  in Fig. 2(f), which is the same as for  $|\alpha = 0\rangle$ ]. Obviously, by doubling the period, this extra global phase does not appear. It was discussed in Ref. [33] that the quasiperiod  $T_d$  of even  $d$  is twice larger than that for odd  $d$ . Nevertheless if one ignores the global  $\pi$  shift (which is usually physically justified) then

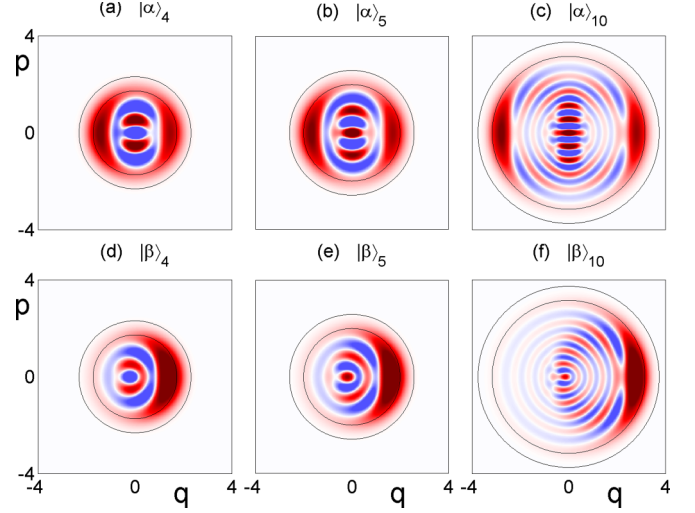


FIG. 6. (Color online) Wigner functions for the qudit CS  $|\alpha\rangle_d$  [(a)–(c)] and  $|\beta\rangle_d$  [(d)–(f)] with  $\alpha = \beta = T_d/2$  for  $d = 4, 5, 10$ , respectively. The corresponding plots for  $d = 2, 3$  are shown in Figs. 2–5 for  $\alpha = \beta = T_d/2$ . The color codes are the same as in Fig. 2. Panels (a), (c), and (b) show the Wigner functions for cat states: the odd ( $|\alpha_{-}\rangle_d$ ) and even ( $|\alpha_{+}\rangle_d$ ) QCS, respectively. We note that  $|\alpha_{\pm}\rangle_d$  are also very close to  $|\beta_{\pm}\rangle_d$  as revealed by their fidelities close to 1, which are shown in Table I. All these Wigner functions are phase sensitive due to quantum interference in phase space.

Eq. (27) determines the quasiperiods of the QCS  $|\alpha\rangle_d$  both for the even and odd dimensions  $d$ .

By analyzing Figs. 2 and 4, one can find that  $W(q, p; |T_d - \alpha\rangle_d)$  is just  $W(q, p; |\alpha\rangle_d)$  but rotated by  $\pi$  in phase space. This can be easily understood by recalling the exact symmetries for  $d = 2, 3$ :

$$\begin{aligned} W(q, p; |T_d - \alpha\rangle_d) &= W(q, p; |-\alpha\rangle_d) \\ &= W(-q, -p; |\alpha\rangle_d). \end{aligned} \quad (28)$$

Analogous approximate symmetries hold for the quasiperiods  $T_d$  with  $d > 3$ . These properties imply that  $W(q, p; |T_d/2\rangle_d)$  are perfectly symmetric [as shown in Figs. 2(c) and 4(c)] or approximately symmetric [see Figs. 6(a)–6(c)] along the line  $q = 0$  in phase space.

The state  $|\alpha\rangle_2$  for  $\alpha = T_2/2$  [as shown in Fig. 2(c)] is just a single-photon Fock state, so it can hardly be considered a real cat state. The simplest nontrivial cat state  $|\alpha = T_d/2\rangle_d$ , as a superposition of the two out-of-phase QCS, exists for  $d = 3$  as given by

$$|\alpha = \frac{1}{2}T_3\rangle_3 = \frac{1}{3}(|0\rangle + 2\sqrt{2}e^{i2\phi_0}|2\rangle), \quad (29)$$

which follows from Eq. (A1).

##### C. Analytical explanation of cat-state generation by displacing vacuum

Here we show that  $|\alpha\rangle_d$  quasiperiodically evolves into the odd (even) QCS for an even (odd) dimension  $d > 3$ . In addition, the *exact* periodic generation of the even QCS  $|\alpha_{+}\rangle_3$  for  $d = 3$  is shown explicitly in the Appendix.

First, by recalling the reflection formula  $\text{He}_n(-x) = (-1)^n \text{He}_n(x)$ , we find that Eq. (6) for even  $n$  (and any  $d$ )

can be rewritten as

$$c_n^{(d)}(\alpha) = 2f_n^{(d)} \sum_{l=1}^{\sigma} \frac{\text{He}_n(x_l)}{[\text{He}_{d-1}(x_l)]^2} \cos(x_l|\alpha|) + \delta_{d,\text{odd}} f_n^{(d)} \frac{\text{He}_n(0)}{[\text{He}_{d-1}(0)]^2}, \quad (30)$$

while for odd  $n$  as

$$c_n^{(d)}(\alpha) = 2if_n^{(d)} \sum_{l=1}^{\sigma} \frac{\text{He}_n(x_l)}{[\text{He}_{d-1}(x_l)]^2} \sin(x_l|\alpha|), \quad (31)$$

where  $\sigma = \text{int}(d/2)$  is the integer part of  $d/2$ ,  $f_n^{(d)}$  is defined by Eq. (7), and  $x_l$  for  $l = 1, \dots, \sigma$  denote only positive roots of  $\text{He}_d(x)$ , contrary to  $x_k$  in Eq. (6) corresponding to all  $d$  roots. The Hermite polynomials in the last term in Eq. (30) can be explicitly given in terms of the Euler  $\Gamma$  function as  $\text{He}_n(0) = \sqrt{\pi} 2^n / \Gamma[(1-n)/2]$ .

Then, we apply oscillatory functions approximating well the Hermite polynomials for small  $|x| \ll \sqrt{2n}$ , which can be given for even  $n$  as follows [68]:

$$\text{He}_n(x) \approx i^n (n-1)!! \exp\left(\frac{1}{4}x^2\right) \cos\left(x\sqrt{n+\frac{1}{2}}\right) \quad (32)$$

and for odd  $n$  as

$$\text{He}_n(x) \approx -i^{n+1} \frac{n!!}{\sqrt{n}} \exp\left(\frac{1}{4}x^2\right) \sin\left(x\sqrt{n+\frac{1}{2}}\right). \quad (33)$$

Thus, it is readily seen from Eqs. (32) and (33) that the roots of  $\text{He}_d(x)$  for  $l = -(d-1), -(d-3), \dots, (d-3), (d-1)$  are

$$x_l^{(d)} \approx \frac{l\pi}{\sqrt{4d+2}}, \quad (34)$$

which results in Eq. (27) for the quasiperiod  $T_d$  of  $|\alpha\rangle_d$  if the global phase of  $|\alpha\rangle_d$  is ignored. Note that in Eqs. (30) and (31), the roots  $x_l^{(d)}$  are considered for positive  $l$  only. Equation (34) also implies that  $x_l^{(d)} T_d/2 \approx l\pi/2$ . Thus, by applying this result to Eqs. (30) and (31), we have (for  $n = 0, 1, \dots$ )

$$c_{2n}^{(2\sigma)}\left(\frac{1}{2}T_{2\sigma}\right) \approx 0, \quad c_{2n+1}^{(2\sigma)}\left(\frac{1}{2}T_{2\sigma}\right) \neq 0, \quad (35)$$

corresponding to the generation of the odd QCS for an even dimension  $d = 2\sigma$ , and

$$c_{2n}^{(2\sigma+1)}\left(\frac{1}{2}T_{2\sigma+1}\right) \neq 0, \quad c_{2n+1}^{(2\sigma+1)}\left(\frac{1}{2}T_{2\sigma+1}\right) \approx 0, \quad (36)$$

which explains the generation of the even QCS for an odd dimension  $d = 2\sigma + 1$ . Finally, we can write

$$|\alpha = \frac{1}{2}T_{2\sigma}\rangle_{2\sigma} \approx |\alpha_-\rangle_{2\sigma} \approx |\beta_-\rangle_{2\sigma}, \quad (37)$$

$$|\alpha = \frac{1}{2}T_{2\sigma+1}\rangle_{2\sigma+1} \approx |\alpha_+\rangle_{2\sigma+1} \approx |\beta_+\rangle_{2\sigma+1}, \quad (38)$$

where the relations for  $|\beta_{\pm}\rangle_d$  are given on the basis of their definitions and our numerical calculations discussed in the next section and summarized in Table I.

#### D. Photon-number distributions and fidelities of the cat-state generation

Figure 7 shows the photon-number distributions for the QCS  $|\alpha\rangle_d$  and  $|\beta\rangle_d$  assuming  $\alpha = \beta$  to be in the middle

TABLE I. Comparison of the fidelities for the QCS  $|\alpha\rangle_d$  and  $|\beta\rangle_d$ , and the corresponding cat states  $|\alpha_{\pm}\rangle_d$  and  $|\beta_{\pm}\rangle_d$  assuming  $\alpha = \beta = T_d/2$  and the sign  $+$  ( $-$ ) is chosen for the odd (even)  $d$ -dimensional Hilbert space. Additionally,  $F_{\text{mix}}^{(d)}$  is given by Eq. (40).

$d$	$ \langle d \alpha \beta\rangle_d ^2$	$ \langle d \alpha \alpha_{\pm}\rangle_d ^2$	$ \langle d \alpha \beta_{\pm}\rangle_d ^2$	$ \langle d \alpha_{\pm} \beta_{\pm}\rangle_d ^2$	$F_{\text{mix}}^{(d)}$
2	0.7116	1.0000	1.0000	1.0000	0.7116
3	0.6580	1.0000	0.9956	0.9956	0.6580
4	0.5788	0.9948	0.9947	0.9998	0.6369
5	0.5616	0.9957	0.9950	0.9993	0.6183
10	0.5341	0.9977	0.9969	0.9993	0.5769
11	0.5317	0.9978	0.9972	0.9993	0.5726
20	0.5206	0.9988	0.9984	0.9996	0.5513
21	0.5199	0.9988	0.9984	0.9996	0.5499
100	0.5076	0.9997	0.9997	0.9999	0.5212
101	0.5075	0.9997	0.9997	0.9999	0.5211

of the quasiperiod  $T_d$  for  $d = 3, 4, 20, 21$ . It is seen that every second term in all these cases of  $|\alpha\rangle_d$  is practically vanishing on the scale of the figures. This is in contrast to the photon-number distribution for  $|\beta\rangle_d$ , which is a truncated Poissonian distribution of the conventional Glauber CS. Thus, Fig. 7 confirms our predictions that  $|\alpha\rangle_d$  corresponds either to even or odd QCS depending on the parity of the dimension  $d$ . It is worth noting that the photon-number oscillations in the QCS  $|\alpha\rangle_d$  are a clear signature of quantum interference in phase space. This can be described even semiclassically in analogy to the explanation of the photon-number oscillations for squeezed states [6,64].

To show how well the QCS can approximate the cat states, we calculate the fidelities between various states, as shown in Table I. As already mentioned, for  $d = 2$  and  $\alpha = \beta = \pi/2$ , the qubit cat states are singular, because they correspond

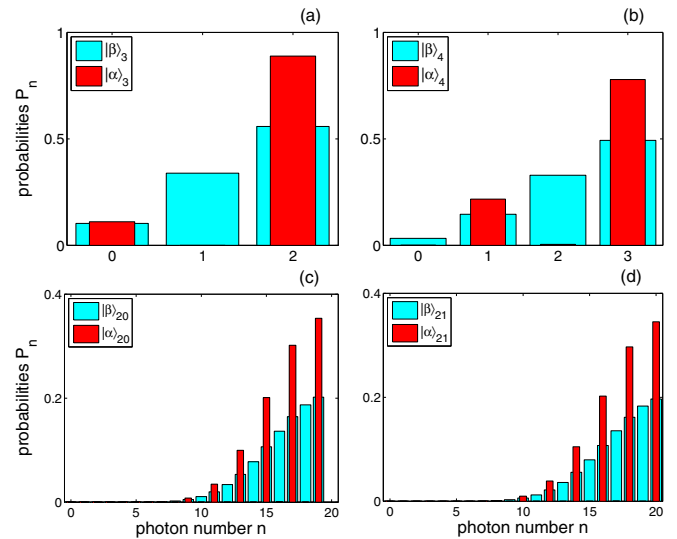


FIG. 7. (Color online) Photon-number distributions  $P_n(\alpha) = |\langle n|\alpha\rangle_d|^2$  (red thin) and  $P_n(\beta) = |\langle n|\beta\rangle_d|^2$  (broad cyan bars) for the QCS  $|\alpha\rangle_d$  and  $|\beta\rangle_d$  with  $\alpha = \beta = T_d/2$  and various  $d$ . It is seen that the Schrödinger cat states are generated: the even QCS  $|\alpha\rangle_d = |\alpha_+\rangle_d$  for (a)  $d = 3$  and (d)  $d = 21$ , while the odd QCS  $|\alpha\rangle_d = |\alpha_-\rangle_d$  for (b)  $d = 4$  and (c)  $d = 20$ .

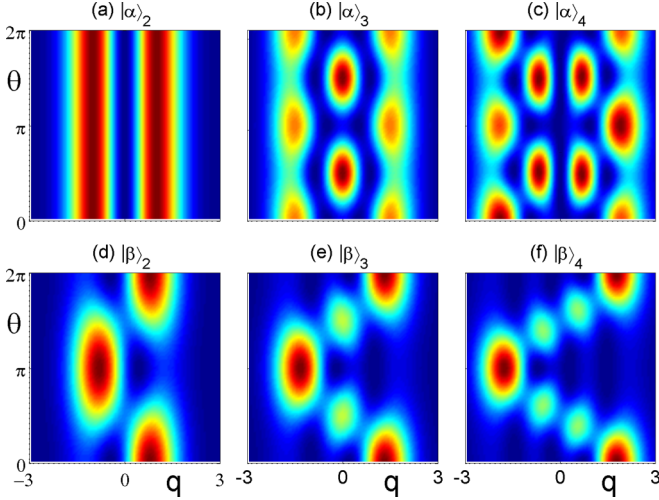


FIG. 8. (Color online) Optical tomograms for the QCS  $|\alpha\rangle_d$  [(a)–(c)] and  $|\beta\rangle_d$  [(d)–(f)] for  $\alpha = \beta = T_d/2$  with  $d = 2, 3, 4$ . Dark blue (dark orange) regions show zero (maximum) values. The upper row tomograms correspond to (a) the single-photon Fock state, (b) the even QCS (the Schrödinger even cat state)  $|\alpha\rangle_3 \approx |\alpha_+\rangle_3 \approx |\beta_+\rangle_3$ , and (c) odd QCS (odd cat state)  $|\alpha\rangle_4 \approx |\alpha_-\rangle_4 \approx |\beta_-\rangle_4$ . The tomograms are  $2\pi$  periodic in  $\theta$ , thus the divided peaks near  $\theta = 0, 2\pi$  should be understood as combined together.

to a single-photon Fock state, i.e.,  $|\alpha\rangle_2 = |\alpha_-\rangle_2 = |\beta_-\rangle_2 = |1\rangle$  [as shown in Figs. 2(c) and 8(a)], which results in the perfect fidelities between these states. The lowest-dimensional nontrivial QCS corresponding to a cat state can be observed for  $d = 3$  and  $\alpha = \beta = T_3/2$ , as we have  $|\alpha\rangle_3 = |\alpha_+\rangle_3$ , given by Eq. (29) [see Figs. 4(c), 7(a), and 8(b)], which is similar but not exactly equal to  $|\beta_+\rangle_3$ . These properties result in  $|\langle\alpha|\alpha_+\rangle_3|^2 = 1$  and  $|\langle\alpha|\beta_+\rangle_3|^2 < 1$ . As already mentioned, there is a perfect periodicity of  $|\alpha\rangle_d$  as a function of  $\alpha$  for  $d = 2, 3$ , and only quasiperiodicity for  $d \geq 4$ .

The lowest fidelities  $|\langle\alpha|\alpha_\pm\rangle_d|^2$  and  $|\langle\alpha|\beta_\pm\rangle_d|^2$  among any dimension  $d$  if  $\alpha = \beta = T_d/2$  are achieved for  $d = 4$  [see Figs. 6(a), 7(b), and 8(c)] as the accuracy of the quasiperiod  $T_4$  of  $|\alpha\rangle_4$  is the worst for this dimension among any finite  $d$ . Nevertheless, this worst case still corresponds to the relatively high fidelities, i.e.,  $|\langle\alpha|\alpha_-\rangle_4|^2 \approx |\langle\alpha|\beta_-\rangle_4|^2 \approx 0.995$ . By contrast, the generated cat states  $|\alpha\rangle_d$  for  $\alpha = T_d/2$  are clearly different from the mixed states

$$\rho_{\text{mix}}^{(d)} = \frac{1}{2}(|\beta\rangle_d \langle\beta| + |-\beta\rangle_d \langle-\beta|) \quad (39)$$

with  $\alpha = \beta$ . This is shown in Table I for the fidelities

$$F_{\text{mix}}^{(d)} = \langle\alpha|\rho_{\text{mix}}^{(d)}|\alpha\rangle_d, \quad (40)$$

which, together with  $|\langle\alpha|\beta\rangle_d|^2$ , are evidently much smaller than the other fidelities listed there.

By analyzing the Wigner functions in Figs. 2 and 4 for increasing  $\alpha$ , one can interpret the state  $|\alpha\rangle_d$  at the midpoint of the quasiperiod  $T_d$  as a result of the interference of a single QCS  $|\alpha\rangle_d$  with its reflection  $|-\alpha\rangle_d$  from the Fock state  $|d\rangle$  at the boundary of the Hilbert space.

### E. Optical tomograms for cat states

The optical tomogram  $w_\psi(q, \theta)$  is the marginal distribution of the Wigner function  $W_\psi(q, p)$  for a given state  $|\psi\rangle$  of the quadrature component  $q$  rotated by angle  $\theta$  in the quadrature phase space [6]:

$$w_\psi(q, \theta) = \int_{-\infty}^{\infty} W_\psi(q \cos \theta - p \sin \theta, q \sin \theta + p \cos \theta) \times dp. \quad (41)$$

Tomograms are directly measurable in homodyne detection, which enable an indirect reconstruction of the Wigner function. So, one can match experiment with theory. This particular feature of tomograms makes them useful. Recently, Filippov and Man'ko [69] obtained a closed form analytic expression for the optical tomogram of any qudit superposition state, given by Eq. (1), as

$$w_\psi(q, \theta) = \frac{e^{-q^2}}{\sqrt{\pi}} \sum_{n=0}^{d-1} \left[ \frac{|c_n|^2}{2^n n!} H_n^2(q) + \frac{|c_n|}{\sqrt{2^n n!}} H_n(q) \times \sum_{k=n+1}^{d-1} \frac{|c_k| \cos[(n-k)\theta - \phi_n + \phi_k]}{\sqrt{2^{k-2} k!}} H_k(q) \right], \quad (42)$$

where  $c_j = |c_j|e^{i\phi_j}$  and  $H_j(q)$  is the Hermite polynomial of degree  $j$  ( $j = n, k$ ). We have used Eq. (42) to obtain tomograms of the QCS  $|\alpha\rangle_d$  and  $|\beta\rangle_d$ .

Figures 8(b), 8(c), and 9 show a few examples of the tomograms for the low-dimensional Schrödinger cat states  $|\alpha = T_d/2\rangle_d$  in comparison to  $|\beta = T_d/2\rangle_d$ . In addition, Fig. 8(a) shows a single-photon state  $|\alpha = T_2/2\rangle_2 = |1\rangle$ , which can be considered a singular “cat” state. It is seen for  $|\beta\rangle_d$  that the tomograms have two main peaks (if the divided peaks at the boundaries for  $\theta = 0$  and  $2\pi$  are combined together) and  $2(d-2)$  smaller peaks, so altogether  $2(d-1)$  peaks. The total number of peaks of the tomograms for  $|\alpha\rangle_d$  in comparison to  $|\beta\rangle_d$ , is more difficult to be estimated for arbitrary  $d$  because, e.g., some peaks are not well separated [e.g., compare the smallest peaks in Figs. 9(a) and 9(b)]. For  $|\alpha\rangle_d$  there are altogether four outermost peaks on the left- and right-hand sides independent of the dimension  $d$ , and a few squeezed peaks between them depending on  $d$ , as clearly seen in Fig. 9. Note that  $|\alpha\rangle_d$  cannot be precisely obtained by simply superimposing the tomograms for  $|\beta\rangle_d$  and  $|-\beta\rangle_d$  (which is a  $\pi$ -rotated tomogram for  $|\beta\rangle_d$ ). This would correspond

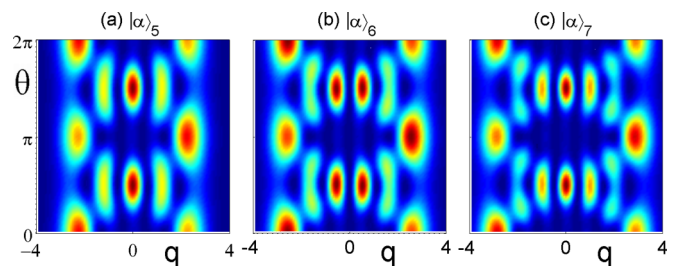


FIG. 9. (Color online) Optical tomograms for the even (for  $d = 5, 7$ ) and odd ( $d = 6$ ) QCS  $|\alpha = T_d/2\rangle_d$ .

to a tomogram for  $\rho_{\text{mix}}^{(d)}$ , given by Eq. (39), for which the corresponding fidelity  $F_{\text{mix}}^{(d)}$ , given by Eq. (40), is quite low, as shown in Table I.

The tomograms for  $|\psi\rangle = |\alpha = T_d/2\rangle_d$  are *approximately* symmetric with respect to reflection along the axes  $q = 0$  and  $\theta = \pi$  (in addition to the symmetry along  $\theta = 0$ ), i.e.,  $w_\psi(q, \theta) \approx w_\psi(-q, \theta)$  and  $w_\psi(q, \pi + \theta) \approx w_\psi(q, \pi - \theta)$ . Only the latter symmetry is observed for  $|\psi\rangle = |\beta = T_d/2\rangle_d$  as seen in Figs. 8(d)–8(f). Note that the imperfections of the symmetries come from the imperfect cat-state generation (i.e.,  $|\alpha\rangle_d$  is not exactly equal to  $|\alpha_\pm\rangle_d$  for  $\alpha = T_d/2$  with  $d > 3$ ) and, more importantly, from the interference in phase space, which means that the tomograms (and the corresponding Wigner functions) of any superpositions of states  $|\alpha\rangle_d$  and  $|\beta\rangle_d$  are more asymmetric than their mixtures.

### F. Nonclassicality of the cat states

A quantum state can be considered *nonclassical* if its Glauber-Sudarshan  $P$  function cannot be interpreted as a classical probability density, i.e., it is nonpositive [70]. In particular, if the  $P$  function is more singular than the Dirac delta function then it is also nonpositive [71]. Thus, any qudit state (including our QCS), which is not the vacuum state, is nonclassical as any finite superposition of Fock states is nonclassical.

There are various measures and criteria (witnesses) of nonclassicality of optical states [70,71]. Formally the best measures are those based directly or indirectly on the  $P$  function. However, due to the singularity of the  $P$  function, they are not operationally useful except for some very special states. Thus, we use an operational parameter (or a quantitative witness) of nonclassicality based on the Wigner function.

Here, in the analysis of the qudit Schrödinger cat states, we apply the nonclassical volume, which is a quantitative parameter of the amount of nonclassicality of a given quantum state based on the Wigner function [41]. In this particular measure, the volume of the negative part of the Wigner function is considered as an indicator (or parameter) of nonclassicality. To be precise, the nonclassical volume is defined as a doubled volume of the integrated negative part of the Wigner function of a quantum state  $|\psi\rangle$  [41]:

$$\delta(|\psi\rangle) = \int_{-\infty}^{\infty} \int_{-\infty}^{\infty} |W_\psi(q, p)| dq dp - 1, \quad (43)$$

where  $W_\psi(q, p)$  is the Wigner function of a quantum state  $|\psi\rangle$ . A nonzero value of  $\delta(|\psi\rangle)$  implies that the given state  $|\psi\rangle$  is nonclassical. For example, the vacuum is a classical state so  $\delta(|0\rangle) = 0$ , while the single-photon Fock state has the nonclassical volume equal to  $\delta(|1\rangle) = 4e^{-1/2} - 2 \approx 0.426$  [41].

By analyzing Fig. 10, which shows the nonclassical volume  $\delta$ , one can conclude that, at least for small  $d$ , the following properties hold: (a)  $\delta(|\alpha = \frac{1}{2}T_{d+1}\rangle_{d+1}) > \delta(|\alpha = \frac{1}{2}T_d\rangle_d)$ , (b)  $\delta(|\beta\rangle_{d+1}) > \delta(|\beta\rangle_d)$  if  $|\beta| \gg 0$ , while (c)  $\delta(|\beta\rangle_{d+1}) < \delta(|\beta\rangle_d)$  if  $|\beta| \approx 0$ , and (d) analogously  $\delta(|\alpha\rangle_{d+1}) < \delta(|\alpha\rangle_d)$  if  $|\alpha| \approx 0$ . Moreover, (e)  $\delta(|\alpha\rangle_d) > \delta(|\beta\rangle_d)$  if  $|\alpha| = |\beta| \leq \frac{1}{2}T_d$ .

It is seen in Fig. 10(a) that  $\delta(|\alpha\rangle_2)$  reaches its maximum value of  $4e^{-1/2} - 2$  for  $\alpha = T_2(n + 1/2)$  with  $n = 0, 1, \dots$ , which corresponds to the generation of the Fock state  $|1\rangle$  [see also Fig. 1(c)]. For higher  $d$ , the local maxima of  $\delta(|\alpha\rangle_d)$  are

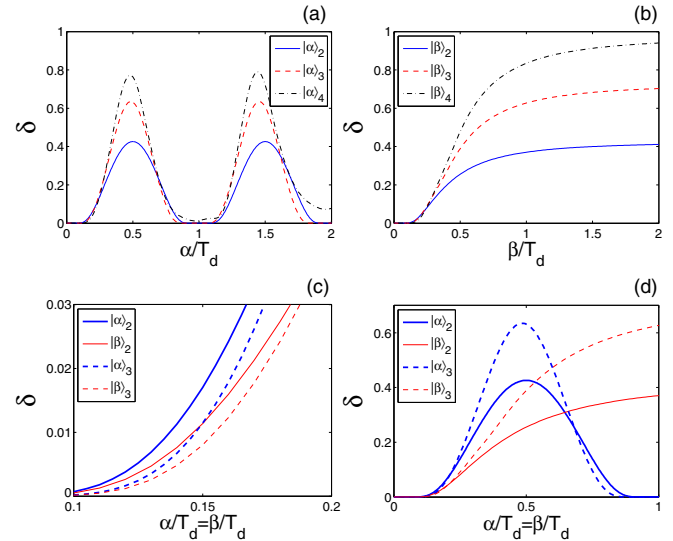


FIG. 10. (Color online) Variation of the nonclassical volume  $\delta(|\psi\rangle)$  with the real amplitudes  $\alpha$  and  $\beta$  as a fraction of the quasiperiods  $T_d$  for the QCS  $|\alpha\rangle_d$  and  $|\beta\rangle_d$  with  $d = 2, 3, 4$ .

also reached for  $\alpha = T_d(n + 1/2)$ , which corresponds to the generation of the even and odd cat states. So, in terms of the nonclassical volume, the most nonclassical QCS  $|\alpha\rangle_d$  for a given  $d$ , are the cat states. This fact also justifies our choice of  $\alpha = T_d/2$  for the construction of the tomograms shown in Figs. 8 and 9.

It is seen in Fig. 10(c) that the range of  $\alpha = \beta$  for which  $\delta(|\alpha\rangle_d) \approx \delta(|\beta\rangle_d) \approx 0$  increases with  $d$ , also as a fraction of  $T_d$ , for both types of QCS. This indirectly shows that these QCS tend to the conventional Glauber coherent states for  $|\alpha| = |\beta| \ll d$ .

These and other quantifiers and witnesses were also analyzed in the context of the generation of standard infinite-dimensional Schrödinger cat states and their quantum-to-classical transition by, e.g., Paavola *et al.* [72]. Their analysis of nonclassicality includes (1) a nonclassical depth based on the  $s$ -parametrized generalization of the Glauber-Sudarshan and Wigner functions, (2) the highest point of the interference fringes of the Wigner function, (3) the Vogel nonclassicality criterion based on the matrices of moments of annihilation and creation operators, and (4) the Klyshko criterion based on the photon-number distribution in addition to (5) the nonclassical volume studied here. Numerous other nonclassicality parameters, which can also be applied in this context, are listed in, e.g., Ref. [71].

## V. CONCLUSIONS

We compared properties of two kinds of qudit (or  $d$ -level) CS: (i)  $|\alpha\rangle_d$  defined by the action of the qudit displacement operator on the vacuum and (ii)  $|\beta\rangle_d$  defined by the Poissonian expansion in Fock states truncated at the state  $|d - 1\rangle$ . In the infinite-dimensional limit of the Hilbert space or, practically, if  $|\alpha| = |\beta| \ll d$ , these two QCS go into the same conventional Glauber CS. Also the states are equivalent for the qubit case (i.e., for  $d = 2$ ). However, for other cases, the QCS  $|\alpha\rangle_d$  and  $|\beta\rangle_d$  exhibit distinctly different properties. The crucial

difference between these two types of QCS is that the state  $|\alpha\rangle_d$  with increasing  $\alpha = \beta$  exhibits periodic (for  $d = 2, 3$ ) or quasiperiodic (for  $d > 3$ ) reflections from the boundary states  $|0\rangle$  and  $|d - 1\rangle$  of the Hilbert space  $\mathcal{H}^{(d)}$ , which we described as multiple bounce or a ping-pong effect. By contrast, the QCS  $|\beta\rangle_d$  is not reflected from the boundaries of the Hilbert space as  $\beta$  increases, which produces no reflections and no bouncing of the Wigner function. Although the quasiperiodicity of the QCS  $|\alpha\rangle_d$  was already discussed in Refs. [33,67], our phase-space description in terms of the standard Wigner function shows these effects especially clearly in terms of quantum interference in phase space.

We have shown analytically that the QCS  $|\alpha\rangle_d$  for  $\alpha = T_d/2$  form macroscopically distinguishable superpositions of two qudit CS. Thus, these Schrödinger cat states can be simply generated by a direct displacement of the vacuum state in a qudit system. The cat states can contain Fock states with only odd or even photon numbers, depending on whether the qudit dimension  $d$  is even or odd, and thus referred to as the odd or even QCS, respectively. We have interpreted this phenomenon as an interference of a single CS  $|\alpha\rangle_d$  with its reflection  $|\alpha\rangle_d$  from the highest-energy Fock state  $|d - 1\rangle$  of the qudit Hilbert space.

Various experimental methods (see, e.g., Refs. [32], and references therein) have been developed for the generation of quantum superpositions of two and more well-separated quasiclassical states of light. In particular, it is well known theoretically, and recently confirmed experimentally [73], that an initial CS in a Kerr medium with the third-order nonlinear susceptibility can evolve into a superposition of two [74–76] or more [77] macroscopically distinct superpositions of infinite-dimensional CS. Also the evolution of an initial coherent state through a Kerr medium, described by a higher-order nonlinear susceptibility, results in the production of Schrödinger cat [75,76,78] states. We note that Schrödinger cat states can also be produced in a microwave cavity field via its coupling to a superconducting qubit in circuit-QED systems [79], which under special conditions can be modeled as a Kerr-type effect.

The generation of finite-dimensional even and odd cat states discussed in this paper corresponds to a completely different effect as based on simple displacements of the vacuum. The Kerr effect, as shown in Fig. 1(a), was used only as an example of the optical method for the Hilbert-space truncation.

It is worth noting that the QCS, for any nonzero  $\alpha$  and  $\beta$ , are not classical, in contrast to their infinite-dimensional counterpart. It is known that any qudit state different from the vacuum is nonclassical because any finite superposition of Fock states is nonclassical, i.e., described by a nonpositive semidefinite Glauber-Sudarshan  $P$  function. However, so far no effort has been made to compare the nonclassical properties of these two types of QCS. Keeping this in mind, here we investigated the differences between the nonclassical properties of the two types of QCS.

We have illustrated the nonclassical properties of the two types of QCS by studying their photon-number statistics and the nonclassical volume of the Wigner function, which is the Kenfack-Życzkowski quantitative parameter of nonclassicality [41].

By showing similarities and clear differences of finite-dimensional (nonclassical) and infinite-dimensional (classical) systems depending on the complex parameters (such as  $\alpha$  and  $\beta$ ) in comparison to the system dimension, one can address fundamental questions of the quantum-to-classical transition.

For the completeness of our phase-space description, we have also presented optical tomograms of the QCS. These tomograms, which are directly measurable in homodyne detection, enable the complete reconstruction of the Wigner function.

We stress that the discussed QCS are not only of fundamental theoretical interest, as they can be generated in optical systems referred to as the linear and nonlinear quantum scissors (see Secs. II and III).

We would like to emphasize that we studied the generation of Schrödinger cat states in a *general* finite-dimensional bosonic system in which the displacement operation can be applied to the ground state of the system. Figure 1 shows just a few examples of optical realizations of such systems often studied in the literature. Although these systems are theoretically appealing because of their formal simplicity, we do not claim that they are the easiest to be realized experimentally, especially when one uses Kerr nonlinearities modeled by a  $d$ -photon anharmonic oscillator, which is required in the system shown in Fig. 1(a) for  $d > 2$ . We are not aware of any direct experimental realization of a pure  $d$ -photon anharmonic oscillator for  $d > 2$ , although this model was used in a number of theoretical works including the classic articles by Yurke and Stoler [74], and Tombesi and Mecozi [76] on the Schrödinger cat generation. By contrast, the system shown in Fig. 1(a) in the special case of Kerr nonlinearity described by the two-photon anharmonic oscillator enables single-photon blockade [47,48], corresponding to the generation of lossy two-dimensional CS  $|\alpha\rangle_2$ . This effect has already attracted much attention and was demonstrated in a number of experiments in cavity- and circuit-QED setups [52–55]. Also the systems shown in Figs. 1(b) and 1(c) were realized experimentally as reported in, e.g., Refs. [80] (according to the experimental proposal of Ref. [65]) and [43], respectively.

We hope that this work can stimulate further interest in finding applications of the QCS in quantum information processing (including quantum teleportation) with qudits and quantum engineering with multiphoton blockades.

## ACKNOWLEDGMENTS

A.M. was supported by the Polish Ministry of Science and Higher Education under Grant No. DEC-2011/03/B/ST2/01903. A.P. thanks the Department of Science and Technology (DST), India, for support provided through the DST Project No. SR/S2/LOP-0012/2010 and he also thanks the Operational Program Education for Competitiveness–European Social Fund project CZ.1.07/2.3.00/20.0017 of the Ministry of Education, Youth and Sports of the Czech Republic. F.N. is partially supported by the RIKEN iTHES Project, MURI Center for Dynamic Magneto-Optics, JSPS-RFBR Contract No. 12-02-92100, Grant-in-Aid for Scientific Research (S), MEXT Kakenhi on Quantum Cybernetics, and the JSPS via its FIRST program.

## APPENDIX: SIMPLE EXAMPLES OF QCS

Here, for clarity, we give two simple examples of the QCS  $|\alpha\rangle_d$ , showing their relation to the cat state generation.

Equation (5) for  $d = 3$  simplifies to the qutrit CS [10]:

$$|\alpha\rangle_3 = \frac{1}{3}[2 + \cos(\sqrt{3}|\alpha|)]|0\rangle + \frac{1}{\sqrt{3}}e^{i\phi_0} \sin(\sqrt{3}|\alpha|)|1\rangle + \frac{\sqrt{2}}{3}e^{2i\phi_0}[1 - \cos(\sqrt{3}|\alpha|)]|2\rangle. \quad (\text{A1})$$

It is seen that the single-photon term exactly vanishes for  $\alpha = T_3/2 = \pi/\sqrt{3}$ , thus this superposition state reduces exactly to the qutrit even CS, given by Eq. (29). The Wigner functions for  $|\alpha\rangle_3$  with various  $\alpha$ , including  $\alpha = T_3/2$ , are shown in Fig. 4.

For  $\alpha = \beta = \gamma = T_3/2$ , one can calculate explicitly that  $|\alpha\rangle_3 \approx [0.33, 0, 0.94]$ ,  $|\pm\beta\rangle_3 \approx [0.32, \pm 0.58, 0.75]$ ,  $|\gamma\rangle_3 \approx [0.22, -0.58, 0.78]$ , and  $|\beta_+\rangle_3 \approx [0.37, 0, 0.93]$ . Thus, it is seen that  $|\alpha\rangle_3 \approx |\alpha_+\rangle_3 \approx |\beta_+\rangle_3$ , which results in the corresponding fidelities  $\approx 1$  (see Table I). This conclusion can be drawn intuitively (but inaccurately) by comparing the Wigner function  $W(q, p; |\alpha\rangle_3)$ , shown in Fig. 4(c), with  $W(q, p; |\beta\rangle_3)$ , shown in Fig. 5(b), roughly superimposed with  $W(q, p; -|\beta\rangle_3)$ , which is  $W(q, p; |\beta\rangle_3)$  but rotated by  $\pi$  in phase space according to Eq. (28). As already mentioned, such superimposing of plots corresponds to the Wigner function of a mixed state  $\rho_{\text{mix}}^{(3)}$ , given by Eq. (39), clearly different from

$|\alpha\rangle_3$  as indicated by the relatively low fidelity  $F_{\text{mix}}^{(3)} = 0.66$  (see Table I).

For  $d = 4$ , from Eq. (5) one obtains the following quartit CS:

$$|\alpha\rangle_4 = \frac{1}{2} \sum_{k=1,2} \left\{ \frac{1}{x_k^2} \cos y_k |0\rangle + \frac{e^{i\phi_0}}{x_k} \sin y_k |1\rangle + (-1)^k \frac{e^{2i\phi_0}}{\sqrt{3}} \cos y_k |2\rangle + (-1)^k \frac{e^{3i\phi_0}}{x_k} \sin y_k |3\rangle \right\}, \quad (\text{A2})$$

where  $x_{1,2} = x_{1,2}^{(4)} = \sqrt{3 \pm \sqrt{6}}$  are the roots of  $\text{He}_4(x)$  and  $y_k = x_k |\alpha|$ . To show that this state for  $\alpha = T_4/2$  is close to the quartit odd CS, it is enough to calculate the contributions of the Fock states  $|0\rangle$  and  $|2\rangle$ , which are  $|\langle 0|\alpha\rangle_4|^2 = 0.0004$  and  $|\langle 2|\alpha\rangle_4|^2 = 0.0048$ . These contributions are clearly negligible, as also shown in Fig. 7(b). The Wigner function and its tomograms for this cat state are shown in Figs. 6(a) and 8(c) in comparison to the cat states generated in the Hilbert spaces of other dimensions.

An explicit calculation for  $\alpha = \beta = \gamma = T_4/2$  leads to  $|\alpha\rangle_4 \approx [0.02, 0.47, -0.07, 0.88]$  [see Fig. 6(a)],  $|\pm\beta\rangle_4 \approx [0.18, \pm 0.38, 0.57, \pm 0.70]$  [see Fig. 6(d)],  $|\gamma\rangle_4 \approx [-0.15, 0.33, -0.68, 0.64]$ , and  $|\beta_-\rangle_4 \approx [0, 0.48, 0, 0.88]$ . Thus, we see that  $|\alpha\rangle_4 \approx |\alpha_-\rangle_4 \approx |\beta_-\rangle_4$  resulting in a fidelity close to 1 (as shown in Table I). This conclusion can be drawn also for other dimensions  $d$  as seen by comparing Figs. 6(a)–6(c) with Figs. 6(d)–6(f), respectively.

- 
- [1] E. Schrödinger, *Naturwissenschaften* **14**, 664 (1926).  
[2] R. J. Glauber, *Phys. Rev.* **130**, 2529 (1963).  
[3] E. C. G. Sudarshan, *Phys. Rev. Lett.* **10**, 277 (1963).  
[4] W. M. Zhang, D. H. Feng, and R. Gilmore, *Rev. Mod. Phys.* **62**, 867 (1990).  
[5] M. Combescure and R. Didier, *Coherent States and Applications in Mathematical Physics* (Springer, Berlin, 2012).  
[6] W. P. Schleich, *Quantum Optics in Phase Space* (Wiley-VCH, Berlin, 2001).  
[7] A. M. Perelomov, *Generalized Coherent States and Their Applications* (Springer, Berlin, 1986).  
[8] V. Bužek, A. D. Wilson-Gordon, P. L. Knight, and W. K. Lai, *Phys. Rev. A* **45**, 8079 (1992).  
[9] L. M. Kuang, F. B. Wang, and Y. G. Zhou, *Phys. Lett.* **183A**, 1 (1993); *J. Mod. Opt.* **41**, 1307 (1994).  
[10] A. Miranowicz, K. Piątek, and R. Tanaś, *Phys. Rev. A* **50**, 3423 (1994).  
[11] T. Opatrny, V. Bužek, J. Bajér, and G. Drobný, *Phys. Rev. A* **52**, 2419 (1995).  
[12] W. Leoński, *Phys. Rev. A* **55**, 3874 (1997); A. Miranowicz, W. Leoński, S. Dyrting, and R. Tanaś, *Acta Phys. Slov.* **46**, 451 (1996).  
[13] M. A. Marchiolli, *Physica A* **319**, 331 (2003).  
[14] V. V. Borzov and E. V. Damaskinsky, *ZNS POMI* **335**, 75 (2006).  
[15] M. Mirzaee, M. Rezaee, and M. A. Jafarizadeh, *Int. J. Theor. Phys.* **46**, 1471 (2007).  
[16] M. Rezaei, M. R. Rezapour, and M. A. Fasihi, *Int. J. Quantum Inf.* **7**, 517 (2009).  
[17] A. Miranowicz, W. Leoński, and N. Imoto, *Adv. Chem. Phys.* **119**, 155 (2001).  
[18] D. T. Pegg and S. M. Barnett, *J. Mod. Opt.* **44**, 225 (1997).  
[19] R. Tanaś, A. Miranowicz, and Ts. Gantsog, in *Progress in Optics*, edited by E. Wolf (Elsevier, Amsterdam, 1996), Vol. 35, p. 355.  
[20] W. Leoński and A. Miranowicz, *Adv. Chem. Phys.* **119**, 195 (2001).  
[21] F. Dell'Anno, S. De Siena, and F. Illuminati, *Phys. Rep.* **428**, 53 (2006).  
[22] W. Leoński and A. Kowalewska-Kudłazyk, *Prog. Opt.* **56**, 131 (2011).  
[23] A. Muthukrishnan and C. R. Stroud, Jr., *Phys. Rev. A* **62**, 052309 (2000).  
[24] T. C. Ralph, K. J. Resch, and A. Gilchrist, *Phys. Rev. A* **75**, 022313 (2007).  
[25] B. P. Lanyon, M. Barbieri, M. P. Almeida, T. Jennewein, T. C. Ralph, K. J. Resch, G. J. Pryde, J. L. O'Brien, A. Gilchrist, and A. G. White, *Nat. Phys.* **5**, 134 (2009).  
[26] I. Bregman, D. Aharonov, M. Ben-Or, and H. S. Eisenberg, *Phys. Rev. A* **77**, 050301(R) (2008).  
[27] G. Yusa, K. Muraki, K. Takashina, K. Hashimoto, and Y. Hirayama, *Nature (London)* **434**, 1001 (2005); Y. Hirayama, A. Miranowicz, T. Ota, G. Yusa, K. Muraki, Ş. K. Özdemir, and N. Imoto, *J. Phys.: Condens. Matter* **18**, S885 (2006).  
[28] F. A. Bonk, R. S. Sarthour, E. T. deAzevedo, J. D. Bulnes, G. L. Mantovani, J. C. C. Freitas, T. J. Bonagamba, A. P. Guimarães, and I. S. Oliveira, *Phys. Rev. A* **69**, 042322 (2004).

- [29] H. Kampermann and W. S. Veeman, *J. Chem. Phys.* **122**, 214108 (2005).
- [30] M. Neeley *et al.*, *Science* **325**, 722 (2009); F. Nori, *ibid.* **325**, 689 (2009).
- [31] V. Bužek and P. L. Knight, in *Progress in Optics*, edited by E. Wolf (Elsevier, Amsterdam, 1995), Vol. 34, p. 1.
- [32] A. Ourjoumtsev, R. Tualle-Brouri, J. Laurat, and P. Grangier, *Science* **312**, 83 (2006); J. S. Neergaard-Nielsen, B. M. Nielsen, C. Hettich, K. Molmer, and E. S. Polzik, *Phys. Rev. Lett.* **97**, 083604 (2006); A. Ourjoumtsev, H. Jeong, R. Tualle-Brouri, and P. Grangier, *Nature (London)* **448**, 784 (2007); H. Takahashi, K. Wakui, S. Suzuki, M. Takeoka, K. Hayasaka, A. Furusawa, and M. Sasaki, *Phys. Rev. Lett.* **101**, 233605 (2008); A. Ourjoumtsev, F. Ferreyrol, R. Tualle-Brouri, and P. Grangier, *Nat. Phys.* **5**, 189 (2009); J. S. Neergaard-Nielsen, Y. Eto, C. W. Lee, H. Jeong, and M. Sasaki, *Nature Photon.* **7**, 439 (2013); B. Vlastakis, G. Kirchmair, Z. Leghtas, S. E. Nigg, L. Frunzio, S. M. Girvin, M. Mirrahimi, M. H. Devoret, and R. J. Schoelkopf, *Science* **342**, 607 (2013).
- [33] T. Opatrný, A. Miranowicz, and J. Bajer, *J. Mod. Opt.* **43**, 417 (1996).
- [34] E. P. Wigner, *Phys. Rev.* **40**, 749 (1932).
- [35] D. F. Styer *et al.*, *Am. J. Phys.* **70**, 288 (2002).
- [36] L. G. Lutterbach and L. Davidovich, *Phys. Rev. Lett.* **78**, 2547 (1997).
- [37] P. Bertet, A. Auffeves, P. Maioli, S. Osnaghi, T. Meunier, M. Brune, J. M. Raimond, and S. Haroche, *Phys. Rev. Lett.* **89**, 200402 (2002).
- [38] A. Vourdas, *Rep. Prog. Phys.* **67**, 267 (2004).
- [39] W. K. Wootters, *Ann. Phys.* **176**, 1 (1987).
- [40] U. Leonhardt, *Phys. Rev. Lett.* **74**, 4101 (1995).
- [41] A. Kenfack and K. Życzkowski, *J. Opt. B* **6**, 396 (2004).
- [42] *J. Mod. Opt.* **44**, No. 11/12 (1997), special issue on *Quantum State Preparation and Measurement*.
- [43] M. Reck, A. Zeilinger, H. J. Bernstein, and P. Bertani, *Phys. Rev. Lett.* **73**, 58 (1994).
- [44] M. Hofheinz, H. Wang, M. Ansmann, R. C. Bialczak, E. Lucero, M. Neeley, A. D. O'Connell, D. Sank, J. Wenner, J. M. Martinis, and A. N. Cleland, *Nature (London)* **459**, 546 (2009).
- [45] Y. X. Liu, L. F. Wei, and F. Nori, *Europhys. Lett.* **67**, 941 (2004).
- [46] G. M. D'Ariano, L. Maccone, M. G. A. Paris, and M. F. Sacchi, *Phys. Rev. A* **61**, 053817 (2000).
- [47] W. Leoński and R. Tanaś, *Phys. Rev. A* **49**, R20 (1994).
- [48] A. Imamoğlu, H. Schmidt, G. Woods, and M. Deutsch, *Phys. Rev. Lett.* **79**, 1467 (1997).
- [49] I. Buluta, S. Ashhab, and F. Nori, *Rep. Prog. Phys.* **74**, 104401 (2011).
- [50] J. Q. You and F. Nori, *Nature (London)* **474**, 589 (2011).
- [51] Z. L. Xiang, S. Ashhab, J. Q. You, and F. Nori, *Rev. Mod. Phys.* **85**, 623 (2013).
- [52] K. M. Birnbaum, A. Boca, R. Miller, A. D. Boozer, T. E. Northup, and H. J. Kimble, *Nature (London)* **436**, 87 (2005).
- [53] A. Faraon, I. Fushman, D. Englund, N. Stoltz, P. Petroff, and J. Vučković, *Nat. Phys.* **4**, 859 (2008).
- [54] A. J. Hoffman, S. J. Srinivasan, S. Schmidt, L. Spietz, J. Aumentado, H. E. Tureci, and A. A. Houck, *Phys. Rev. Lett.* **107**, 053602 (2011).
- [55] C. Lang *et al.*, *Phys. Rev. Lett.* **106**, 243601 (2011).
- [56] L. Tian and H. J. Carmichael, *Phys. Rev. A* **46**, R6801 (1992); M. J. Werner and A. Imamoğlu, *ibid.* **61**, 011801 (1999); R. J. Brecha, P. R. Rice, and M. Xiao, *ibid.* **59**, 2392 (1999); J. Kim, O. Bensen, H. Kan, and Y. Yamamoto, *Nature (London)* **397**, 500 (1999); S. Rebić, S. M. Tan, A. S. Parkins, and D. F. Walls, *J. Opt. B* **1**, 490 (1999); S. Rebić, A. S. Parkins, and S. M. Tan, *Phys. Rev. A* **65**, 063804 (2002).
- [57] A. Miranowicz, M. Paprzycka, Y. X. Liu, J. Bajer, and F. Nori, *Phys. Rev. A* **87**, 023809 (2013).
- [58] W. Leoński and A. Miranowicz, *J. Opt. B* **6**, S37 (2004); A. Miranowicz and W. Leoński, *J. Phys. B* **39**, 1683 (2006); A. Kowalewska-Kudłaszyk, W. Leoński, and J. Peřina, Jr., *Phys. Rev. A* **83**, 052326 (2011).
- [59] Y. X. Liu, A. Miranowicz, Y. B. Gao, J. Bajer, C. P. Sun, and F. Nori, *Phys. Rev. A* **82**, 032101 (2010).
- [60] N. Didier, S. Pugnetti, Y. M. Blanter, and R. Fazio, *Phys. Rev. B* **84**, 054503 (2011).
- [61] D. T. Pegg, L. S. Phillips, and S. M. Barnett, *Phys. Rev. Lett.* **81**, 1604 (1998).
- [62] A. Miranowicz, *J. Opt. B: Quantum Semiclassical Opt.* **7**, 142 (2005); A. Miranowicz, S. K. Özdemir, J. Bajer, M. Koashi, and N. Imoto, *J. Opt. Soc. Am. B* **24**, 379 (2007).
- [63] J. P. Dowling, W. P. Schleich, and J. A. Wheeler, *Ann. Phys.* **503**, 423 (1991).
- [64] W. Schleich and J. A. Wheeler, *Nature (London)* **326**, 574 (1987).
- [65] Ş. K. Özdemir, A. Miranowicz, M. Koashi, and N. Imoto, *Phys. Rev. A* **64**, 063818 (2001).
- [66] M. Koniorczyk, Z. Kurucz, A. Gábris, and J. Janszky, *Phys. Rev. A* **62**, 013802 (2000).
- [67] W. Leoński, A. Miranowicz, and R. Tanaś, *Laser Phys.* **7**, 126 (1997).
- [68] J. Spanier and K. B. Oldham, *An Atlas of Functions* (Hemisphere, Washington/Springer, Berlin, 1987).
- [69] S. N. Filippov and V. I. Man'ko, *Phys. Scr.* **83**, 058101 (2011).
- [70] W. Vogel and D. G. Welsch, *Quantum Optics* (Wiley-VCH, Weinheim, 2006).
- [71] A. Miranowicz, M. Bartkowiak, X. Wang, Y. X. Liu, and F. Nori, *Phys. Rev. A* **82**, 013824 (2010).
- [72] J. Paavola, M. J. W. Hall, M. G. A. Paris, and S. Maniscalco, *Phys. Rev. A* **84**, 012121 (2011).
- [73] G. Kirchmair, B. Vlastakis, Z. Leghtas, S. E. Nigg, H. Paik, E. Ginossar, M. Mirrahimi, L. Frunzio, S. M. Girvin, and R. J. Schoelkopf, *Nature (London)* **495**, 205 (2013).
- [74] B. Yurke and D. Stoler, *Phys. Rev. Lett.* **57**, 13 (1986).
- [75] G. J. Milburn, *Phys. Rev. A* **33**, 674 (1986).
- [76] P. Tombesi and A. Mecozzi, *J. Opt. Soc. Am. B* **4**, 1700 (1987).
- [77] A. Miranowicz, R. Tanaś, and S. Kielich, *Quantum Opt.* **2**, 253 (1990); R. Tanaś, Ts. Gantsog, A. Miranowicz, and S. Kielich, *J. Opt. Soc. Am. B* **8**, 1576 (1991).
- [78] M. Paprzycka and R. Tanaś, *Quantum Opt.* **4**, 331 (1992).
- [79] Y. X. Liu, L. F. Wei, and F. Nori, *Phys. Rev. A* **71**, 063820 (2005); S. Ashhab and F. Nori, *ibid.* **81**, 042311 (2010).
- [80] S. A. Babichev, J. Ries, and A. I. Lvovsky, *Europhys. Lett.* **64**, 1 (2003).